



# GNSS-Reflectometry: Forest canopies polarization scattering properties and modeling

Xuerui Wu<sup>a,b,c,\*</sup>, Shuanggen Jin<sup>a</sup>

<sup>a</sup> Shanghai Astronomical Observatory, Chinese Academy of Sciences, Shanghai 200030, China

<sup>b</sup> Department of Environment Resources and Management, Chifeng College, Chifeng 024000, China

<sup>c</sup> State Key Laboratory of Remote Sensing Science, Jointly Sponsored by the Institute of Remote Sensing Applications of Chinese Academy of Sciences and Beijing Normal University, Beijing 100859, China

Available online 11 February 2014

## Abstract

Nowadays, GNSS-Reflectometry (GNSS-R) can be a new promising remote sensing tool in the ocean, snow/ice and land surfaces, e.g., vegetation biomass monitoring. Although GNSS-R provides a potentially special L-band multi-angular and multi-polarization measurement, the theoretical vegetation scattering properties and mechanisms for GNSS-R are not understood clearly. In this paper, the GNSS-R vegetation polarization scattering properties are studied and modeled at different incidence angles (specular direction). The bistatic scattering model Bi-mimics is employed, which is the first-order radiative transfer equation. As a kind of forest stand, the Aspen's crown layer is composed of entire leaves, and its parameters in Mimics handbook are used as model input. The specular circular polarizations (co-polarization RR and cross-polarization LR) are simulated. For cross-polarization, the received polarization is assumed as a linear (horizontal and vertical) polarizations and  $\pm 45^\circ$  linear polarizations. Therefore, the HR VR, +45R and -45R polarizations are simulated here. Contributions from different scattering components at RR, LR and VR polarization are also presented. For co-polarization, it is large in the whole specular angles (10–80°). The scattering trends of the other cross polarization (HR, LR, +45R and -45R) are a little similar when compared to the RR and RV. Therefore, the RHCP and V polarizations are more favorable to collect the reflected signals. The trunk heights and crown depths do not affect the scattering trends of RR, RV and RL, while the trunk height has some effect on the scattering amplitude of different polarizations. The azimuth angle has more effects on RR, RL and RV scattering, especially in lower than 50°. The observation angles and polarization combinations are extremely important for GNSS-R remote sensing. © 2014 COSPAR. Published by Elsevier Ltd. All rights reserved.

**Keywords:** GNSS-R; Forest canopy; Scattering; Polarization; Specular

## 1. Introduction

Global Navigation Satellite Systems (GNSS) include the United States' GPS, Europe's Galileo, Russia's GLONASS and China's Beidou. They are originally exploited for

navigation, positioning and timing. GNSS-Reflectometry (GNSS-R) is a new promising remote sensing tool (Gleason et al., 2009; Jin and Komjathy, 2010; Jin et al., 2011; Cardellach et al., 2011), which was first suggested in the early 1993 as a source of opportunity for altimetric measurements (Martin-Neira, 1993). Since then many different applications of GNSS-R have been performed and tested. Most previous works considered the altimetric mode, estimating the delay between direct and reflected signals. However, its scatterometric mode is also very important, i.e., monitoring the targets' properties from their reflected signals. Nowadays, its applications are increasing,

\* Corresponding author at: Shanghai Astronomical Observatory, Chinese Academy of Sciences, Shanghai 200030, China; Department of Environment Resources and Management, Chifeng College, Chifeng 024000, China. Tel.: +86 021 34775291.

E-mail addresses: [xueruiwu@126.com](mailto:xueruiwu@126.com), [xueruiwu@hotmail.com](mailto:xueruiwu@hotmail.com) (X. Wu), [sgjin@shao.ac.cn](mailto:sgjin@shao.ac.cn) (S. Jin).

including the ocean, land and snow/ice surfaces. Furthermore, using GNSS-R's scatterometric mode for land surfaces, remote sensing of soil moisture and vegetation biomass is feasible (Rodriguez-Alvarez et al., 2011a,b; Egido et al., 2012).

Due to strong attenuation and scattering of vegetation, it is difficult to retrieve the soil moisture. However, vegetation biomass monitoring plays an important role in carbon cycle, greenhouse inventories, et al. Compared with the traditional active and passive remote sensing techniques, such as SAR and radiometry, GNSS-R provides a new complementary technique with its unique advantages of small volume, light weight, low power consumption and high time/spatial resolution. Nowadays, Rodriguez-Alvarez et al. (2011a,b) have been using the ground-based SMIGOL-Reflectometer instrument (the Soil Moisture Interference pattern GNSS Observations at L-band Reflectometer) for geophysical parameters retrieval. The Interference Pattern Technique (IPT) is used to measure the fluctuations of the direct signals due to the multipath generated by the reflected interference signals. The minimum amplitude oscillation is called as notch and its number and position are a function of soil moisture and vegetation height (Rodriguez-Alvarez et al., 2011a,b). Small et al. (2010) estimated the vegetation growth qualitatively using the multipath information of GPS stations at Plate Boundary Observatory (PBO) network and found that NDVI (Normalized Difference Vegetation Index) is negative correlated to multipath amplitude. Since few GPS stations are set up in the forested area, this method is applicable for crop land, grassland and shrub land, and unsuitable for forest zone.

Ferrazzoli et al. (2010) presented some scattering theoretical simulations using the electromagnetic model developed at Tor Vergata University. Scattering in the specular direction at circular polarization was performed. As for the GNSS-R configuration, vegetation theoretical response showed a deceasing trend with increasing biomass, without showing the typical saturation of radar backscattering measurements. They concluded that forest biomass retrieval was theoretically applicable. Wu et al. (2012a) performed some theoretical simulations using the modified Bi-mimics model for GNSS-R forest and crop biomass study (Wu et al., 2012b) and confirmed its feasibility. But the scattering response to the vegetation biomass needs to further study, especially its polarimetric properties.

Different from the traditional linear microwave remote sensing technique, GNSS transmit the signals of RHCP to mitigate ionospheric effects. After reflecting from the Earth surface, the signals' original correlation function is changed and no longer a regular triangle. Meanwhile, the reflected signals' polarization properties are reversed (Zavorotny and Voronovich, 2000a). The reflected signals' polarization properties are needed to be investigated and analyzed. As it is well known, polarization behavior of electromagnetic waves has the potential utility for various geophysical detections in remote sensing, such as soil moisture, vegetation biomass, surface topography. It is related to the orientation, shape and dielectric properties

of targets. However, the effect of land surface on GNSS-R polarization is not well understood.

As early in Year 2000, Zavorotny and Voronovich (2000a) pointed out the reflected signals' polarization problems at ocean surface. Compared with the RHCP scattering component, the LHCP component was much higher at steep and moderate elevation angles and both components started to converge for low-grazing incidence angles (Zavorotny and Voronovich, 2000a). Models used in the simulations were the local Fresnel Reflectivity (Zavorotny and Voronovich, 2000a) and the Small-Slope Approximation (Zavorotny and Voronovich, 1999). For the ocean part, Clarizia et al. (2012) found a significant difference between the DDMs (delay-Doppler maps) of the UK-DMC satellite data and the Z-V model (Zavorotny-Voronovich), and they carried out simulations of L-band bistatic scattering returns from the ocean surface. The Facet Approach was used to represent polarization effects. It was found that the dominant scattering component from the wave troughs was HH.

Cardellach et al. (2011) mentioned that the received scattering co-polarization components did not agree well with the modeled waveforms. Therefore, the co-polarization scattering component modeling must be investigated. For the land part, the modified DMR was used in the SMEX02 and SMEX03 airborne GPS-R experiments. To receive the reflected signals, only a LHCP antenna was configured with incidence angles from 15° to 35°. Multiple polarizations (linear and circular) were also considered in the BAO tower experiment (Zavorotny and Voronovich, 2000b) to exclude roughness effects and retain the dielectric effects. However, the real data did not support their original hypothesis. In a certain respect, the scattering properties of soil needs carefully study.

The experimental studies found that if LHCP was used, the angular information was masked in the horizontal polarization (Rodriguez-Alvarez et al., 2009, 2011a). Therefore a vertically polarized antenna was used in their ground-based receiver. Unfortunately, no detailed analysis from the physical scattering mechanism was carried out for this antenna polarization configuration. Although the Fresnel reflection coefficients are often used at the present work, this simple scattering model can only account for the smooth surface, which is almost inadequate for the practical random rough surface. However, an accurate description of microwave scattering mechanisms is very important in remote sensing data interpretation, data simulation, quantitative inversion algorithms, and new sensors' design. When considering antenna polarization matching, the polarization of antenna should be sensitive to the observed parameters in order to minimize the polarization loss and maximize the reflected signals. This seems much more important for the weak GNSS reflected signals. This paper focuses on the forest canopy physical scattering mechanism of GNSS-R polarimetric signals. The first-order radioactive transfer equation Bi-mimics model is used (Liang et al., 2005). After the modifications of wave synthesis, it will calculate any transmit and receive signal

polarization. The Aspen, which is composed of trunks and leaves, in the Mimics (the Michigan Microwave Canopy Scattering Model) handbook (Ulaby et al., 1990) is used as the model input, since it is a kind of common representations of the deciduous trees. Theoretical scattering simulations are carried out for co-polarization and cross-polarization signals analysis.

## 2. Scattering models

### 2.1. Mimics model

The Mimics model is a radar backscattering model suitable for forest canopies (Ulaby et al., 1990). Its applicable frequency range is 0.5–10 GHz and the incidence angle should be larger than 10° and lower than 90°. The forest canopy is divided into three layers, the crown layer (C), the trunk layer (T) and the ground layer (G), as shown in Fig.1. All the three components are treated as single scatterers. The forest crown layer is composed of leaves, needles and branches; the trunk layer is composed of the vertically orientated trunks. As for the ground layer, the surface roughness is represented by root mean square height and correlation length. The Mimics model is the first-order solution of the radiative transfer equation. The first-order means that the scattering process involving single scattering is by each layer; the double scattering is by pairs of each layer. Extinction and phase matrices are used to describe the changes of propagating microwave intensity in the layers. There are seven scattering mechanisms in the Mimics model. For more details please refer to the handbook (Ulaby et al., 1990).

### 2.2. Bi-mimics model

In addition to the seven scattering mechanisms (measured in bistatic directions) described in the Mimics model (Ulaby et al., 1990), the ground reflection in the specular direction is included in the Bi-mimics model. The scattering mechanisms are shown in Fig.1. The original Mimics model was a bistatic scattering (Ulaby et al., 1990). As for incidence intensity  $I_i$ ,  $(\theta_i, \varphi_i)$  is the incidence zenith and azimuth angles respectively, while  $(\theta_s, \varphi_s)$  is the scattering zenith and azimuth angles and the scattering intensity is represented by  $I_s$ . In the Bi-mimics model, the incidence intensity and the scattering intensity is related by the first-order bistatic transformation matrix  $T$  (Liang et al., 2005; Ulaby et al., 1990).

$$I_s(\theta_s, \varphi_s) = T(\theta_s, \varphi_s)I_i(\theta_i, \varphi_i) \quad (1)$$

$T$  is given in terms of the extinction and phase matrices, which can be calculated by the average modified Mueller matrices (Liang et al., 2005; Ulaby et al., 1990).

Compared with the Mimics model, the scattering zenith and azimuth angles should be added to implement the Bi-mimics model. Therefore the corresponding angles of extinction and phase matrices for crown, trunk and ground

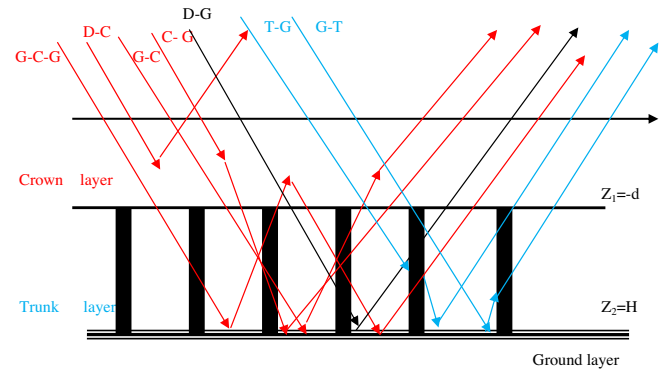


Fig. 1. Scattering mechanisms in the first-order Bi-mimics model, including G–C–G (ground reflection and crown scattering and ground reflection), C–G (crown scattering and ground reflection), DC (direct crown bistatic scattering), G–C (ground reflection and crown scattering), G–T (ground reflection and trunk scattering), DG (direct ground), and T–G (trunk scattering and ground reflection). The specular ground reflection is not shown in the figure. Crown layer depth  $Z_1 = d$ , trunk layer depth  $Z_2 = H$ .

layer should all be modified (Liang et al., 2005). The Mimics model (Ulaby et al., 1990) was originally planned to be developed in three stages. The Mimics model of version 1.5 was used in our work as the basic model. According to the methods mentioned in Liang et al. (2005) and the mimics handbook (Ulaby et al., 1990), the Bi-mimics model was performed by the corresponding modification of Mimics model.

### 2.3. Wave synthesis

The Bi-mimics is a full polarimetric scattering model that incorporates any transmit and receive polarizations (Ulaby et al., 1990). The following wave synthesis equation (Eq. (2)) gives the bistatic scattering cross section.

$$\sigma_{rt}(\psi_r, \chi_r, \psi_t, \chi_t) = 4\pi \tilde{Y}_m^r M_m Y_m^t \quad (2)$$

where  $(\psi_r, \chi_r)$ ,  $(\psi_t, \chi_t)$  are the orientation and ellipticity angles for receive and transmit polarizations, respectively.  $M_m$  is the  $4 \times 4$  real modified Mueller matrix (Ulaby and Elachi, 1990). The modified Stokes vectors  $Y_m^t$  and  $Y_m^r$  are given below (Ulaby and Elachi, 1990):

$$Y_m^t = \begin{bmatrix} \frac{1}{2}(1 + \cos 2\psi_t \cos 2\chi_t) \\ \frac{1}{2}(1 - \cos 2\psi_t \cos 2\chi_t) \\ \sin 2\psi_t \cos 2\chi_t \\ \sin 2\psi_t \end{bmatrix} \quad Y_m^r = \begin{bmatrix} \frac{1}{2}(1 + \cos 2\psi_r \cos 2\chi_r) \\ \frac{1}{2}(1 - \cos 2\psi_r \cos 2\chi_r) \\ \sin 2\psi_r \cos 2\chi_r \\ \sin 2\psi_r \end{bmatrix} \quad (3)$$

Using the normalized Stokes vectors of  $Y_m^t$  and  $Y_m^r$ , the corresponding polarization scattering cross sections can be calculated.

### 2.4. Specular scattering

The reflected signals are composed of coherent and incoherent components. As for ocean part, its surface

roughness scales are commonly equivalent to or larger than GNSS wavelength ( $\lambda \approx 19$  cm). Therefore the received power is mainly noncoherent scattering coming from the glistening zone. But as for land surface, its surface roughness scales are well below the GNSS wavelength. Therefore, the receiving power is considered to be the coherent scattering component coming from the first Fresnel Zone (Ferrazzoli et al., 2010; Beckmann and Spizzichino, 1987) and the scattering at the specular direction is much larger.

When the height of receiver is much lower than the height of transmitter, the size of the first Fresnel zone is influenced by the incidence angles and the receiver height. Its shape is an ellipse (Ferrazzoli et al., 2010; Beckmann and Spizzichino, 1987).

As for GNSS-R vegetation remote sensing, the specular scattering ( $\theta_s = \theta_i, \varphi_s = \varphi_i = 0^\circ$ ) should be studied. For one thing, the angles in Bi-mimics can be set as specular directions for calculation. For another, the corresponding extinction and phase matrices should be modified after setting their specular directions. Therefore, the Spec-mimics model is developed for specular scattering calculations. Its scattering mechanisms are the same with the Bi-mimics model (Liang et al., 2005).

### 2.5. Model verification

Currently, the bistatic and forward scattering measurements are not available, but the backscattering Mimics model has already been tested by monostatic radar experimental data. Liang et al. (2005) compared the backscattering cross section simulated by Bi-mimics with the original Mimics model (Ulaby et al., 1990). As for the same model inputs, both models provided the same results of backscattering cross section, since the backscattering direction is a special kind of bistatic scattering. As for the circular scattering cross sections, the modified stokes vectors are set to linear to compare with the original linear Bi-mimics model and the Bi-mimics's scattering angles are set in specular ones to compare with the specular scattering cross section calculated by Spec-mimics. Of course, their results are the same for the same model inputs. Although the model has not been validated by the experimental data, the backscattering Mimics model has been verified experimentally over the past years and has been accepted as an efficient canopy backscattering model. Therefore, the consistency between the modified model and the original Mimics model make it (the modified model) believable (Liang et al., 2005). After the modifications of wave synthesis, the Spec-mimics model can be used as an analysis tool. Therefore, the XR polarization scattering coefficient can be calculated, where  $R$  indicates RHCP transmitted, and  $X$  indicates any other polarization received, such as RHCP, LHCP, H, V and  $\pm 45^\circ$  linear polarization. The following sections will illustrate some simulations of different polarizations.

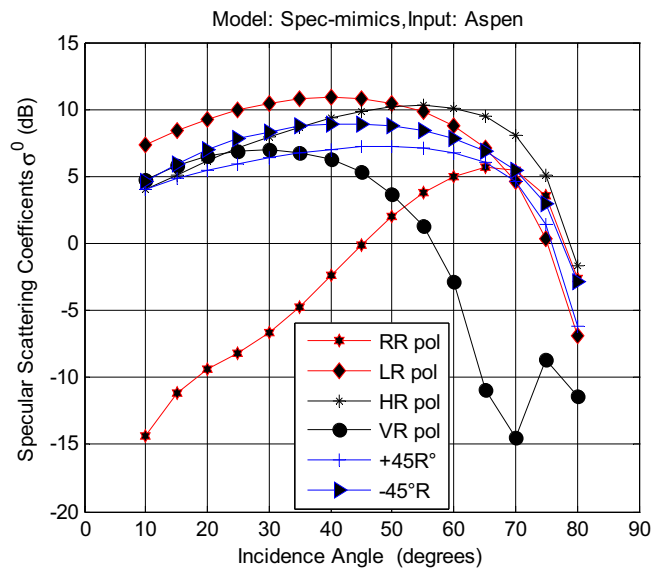


Fig. 2. Specular scattering at XR polarizations vs. incidence angles.

## 3. Forest canopies polarization properties at the specular direction

### 3.1. Circular polarization

Cardellach et al. (2011) stated that the co-polarization component weekly matched the modeled waveforms, which should be included in the model. Fig. 2 shows the co-polarization (RR) and cross-polarization (RL) scattering versus incidence angles. The co-polarization (RR) scattering is an important component throughout the entire incidence angles range  $10\text{--}80^\circ$ . Scattering at RR polarization is lower than the other XR polarizations ( $\theta \leq 50^\circ$ ), and increases as  $50^\circ < \theta \leq 70^\circ$ . The VR increases slowly in smaller than  $30^\circ$  and then decreases slowly with the increase of incidence angles ( $30^\circ < \theta \leq 40^\circ$ ), but the scattering trend of VR decreases sharply as the increase of incidence angles ( $40^\circ < \theta \leq 70^\circ$ ). There are apparent dips for VR at the incidence angle of  $70^\circ$  and  $80^\circ$ . The scattering dynamics of RR and VR are much larger than the other polarizations (LR, HR,  $+45^\circ R$ ,  $-45^\circ R$ ).

### 3.2. Other cross polarizations

This section will focus on the scattering simulations of different XR polarizations. In order to compare between different polarizations, RR and LR are also presented in Fig. 2. We can see that XR polarizations exist at the entire incidence angles. At smaller incidence angles ( $\theta \leq 40^\circ$ ), the scattering of RR polarization is much lower than any other polarizations. In other words, if  $\theta \leq 40^\circ$ , then  $LR > VR > RR$ . It is assumed that the GNSS-R receiver can receive the reflected signals in the above mentioned observation geometry (the specular observation elevation angle range from  $10^\circ$  to  $80^\circ$ ). The polarization mismatch between the antenna and the reflected signals would make the antenna's

polarization loss larger and the antenna should be chosen according to the polarization, Whereas the dynamic ranges of the RHCP and V are larger and their scattering trends are very different. Therefore, it is much favorable if the RHCP and V polarizations are used for the antenna polarizations as collecting the GNSS-R reflected signals. These various polarizations would be appropriate for the Aspen stand.

### 3.3. Component contributions to the total scattering

Here, we present the component contributions to the total scattering at RR, LR and VR polarizations. The total scattering and the scattering component of the total crown, total trunk, direct-ground, and specular ground are illustrated in Figs. 3–5. As for the total crown part, it includes the C–G component, G–C component and G–C–G component. T–G and G–T components are included in the total trunk layer part. Detail information of the scattering mechanisms please refer to Liang et al. (2005) and Ulaby et al. (1990). As for RR polarization, the different component contributions to the total specular scattering are shown in Fig. 3. From the simulations shown in Fig. 3, it can be seen that the total scattering is dominated by the total trunk layer scattering component and then the S–G (specular ground scattering) component. The D–G scattering (direct ground) is lower than S–G scattering and scattering from crown layer is relatively small ( $20^\circ \leq \theta \leq 75^\circ$ ).

As for LR polarization, the total crown layer scattering exists for the entire incidence angles as shown in Fig. 4, but it is not the dominant one. The total scattering is dominated by the trunk layer. The total trunk component, specular-ground and the direct-ground components also exist at these incidence angles and their contributions decrease in order (the scattering amplitude of the total trunk component is larger than the specular-ground one, which is larger than the direct-ground component). Note that as

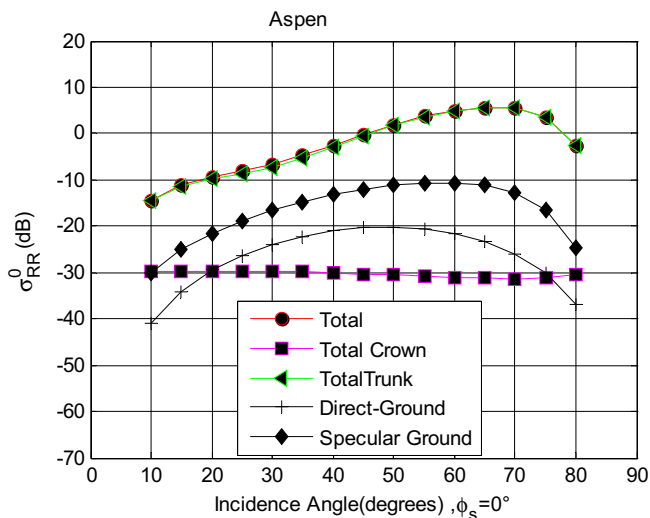


Fig. 3. RR polarization scattering component contributions vs. incidence angles.

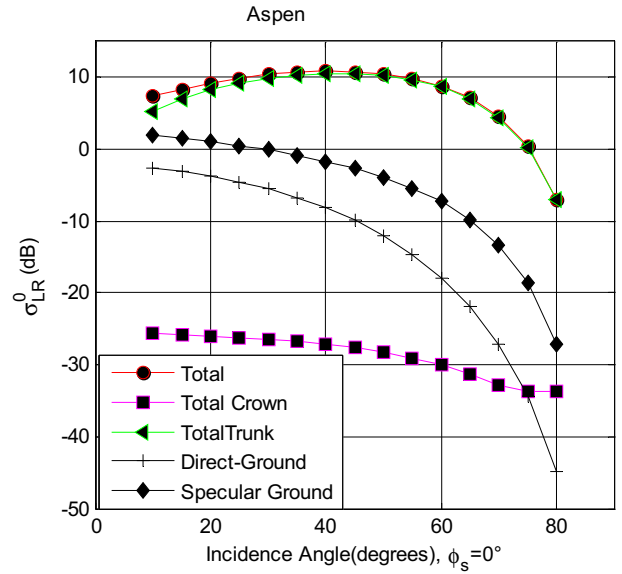


Fig. 4. LR polarization scattering component contributions vs. incidence angles.

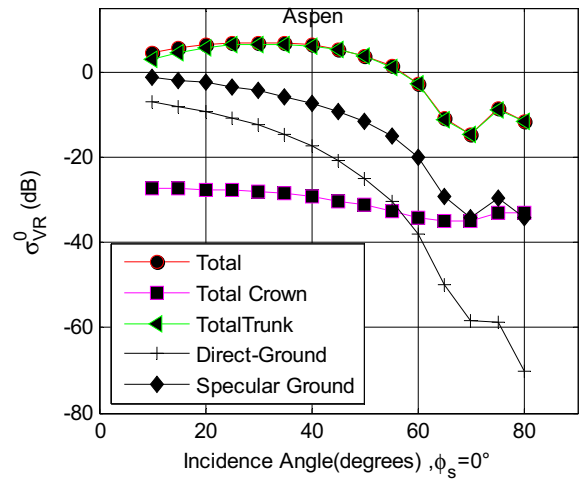


Fig. 5. VR polarization scattering component contributions vs. incidence angles.

for Aspen, there is strong scattering at specular direction due to trunk. However, the crown component contributions exist for the entire incidence angle range, but its scattering amplitudes are the smallest, although the D–G component is the smallest at very large incidence angles ( $\theta \geq 75^\circ$ ).

From Fig. 5, we can see that for VR polarization the total scattering is dominated by the total trunk scattering and both of them (total scattering and the total trunk scattering) exist at the whole incidence angles. The second influencing component to the total scattering is the specular ground component, and its trend is the same with the total scattering component. The direct-ground component is lower than the specular-ground component. When the incidence angles are between  $10^\circ$  and  $50^\circ$ , the total crown component produces the smallest contribution to the total scattering component. But when the incidence angles are

between  $55^\circ$  and  $80^\circ$ , the total crown component is larger than the direct-ground component but lower than the specular-ground component.

### 3.4. Discussion

The previous simulations are for Aspen, which has vertical orientated trunk layer. The single scatter of a trunk has strong scattering in the specular direction. Other kinds of vegetation scattering in the specular direction should also be carried out to determine the vegetation scattering. But at least for vegetation like Aspen, the above simulations indicate the polarization respond at XR polarizations.

The receiver used in SMEX02 and SMEX03 (Masters et al., 2004) airborne experiment is the modified DMR receiver. It was programmed to track signals from the highest elevation angle in view; therefore its incidence angles are from  $15^\circ$  to  $35^\circ$ . A zenith-orientated RHCP receiving antenna was used to receive direct signals, while a nadir-orientation LHCP receiving antenna was used to receive the reflected signals. The LR is the largest at these incidence angles, while the RR is the smallest. But for larger incidence angles ( $\theta \geq 55^\circ$ ), the RV is the smallest, there are dips, and the scattering trend of RV is very different from the other polarizations. As for larger incidence angles, co-polarization RR and cross polarization will yield more information for vegetation detection. This polarization may provide additional information for other geophysical parameters. Our next work will focus on bare soil and crop polarization study. We hope to find the best polarization and angular combinations for GNSS-R observation and then fully exploit its polarization and angular information for robust remote sensing.

### 4. Sensitivity analysis

We set different trunk heights and crown depths at RR, RL and RV polarization, and calculate the specular scattering analysis. Also, scattering azimuth angles effects are carried out in this section.

From Fig. 6, we can see that the trunk height only affects the amplitudes of the specular scattering coefficients at RR, RL and RV pol. That is to say, the scattering trends are the same for the same polarizations. For RR, RV and RL pol, larger trunk heights correspond to higher scattering at the same incidence angle.

Fig. 7 shows that the effects of crown depths ( $d$ ) on the specular scattering at different polarizations are very small, in fact, less than 2 dB. Since the specular scattering are more sensitive to the forest biomass, which is dominated by the trunk layer.

At present, the common GNSS-R scattering are focusing on the in-plane ( $\varphi_i = \varphi_s$ ) specular scattering, which is the coherent scattering. But the geometry of the GNSS constellations are changing, the ranges of their azimuth angles are  $0\text{--}360^\circ$ . Although it is shown that the coherent

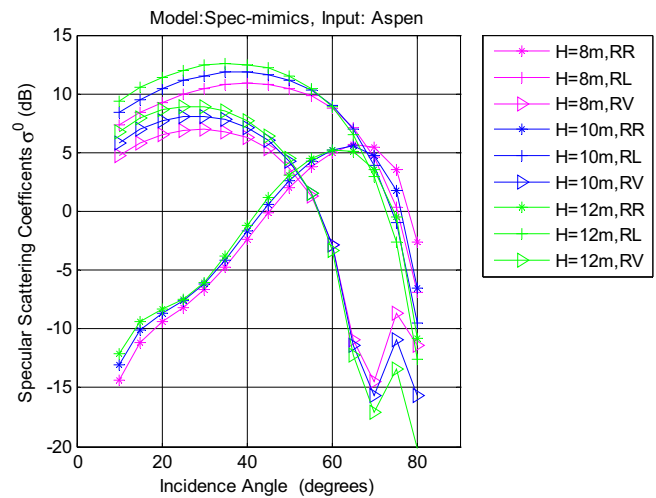


Fig. 6. Specular scattering coefficients of different polarizations (RR, RL and RV) vs. specular incidence angles at different trunk heights (8, 10 and 12 m).

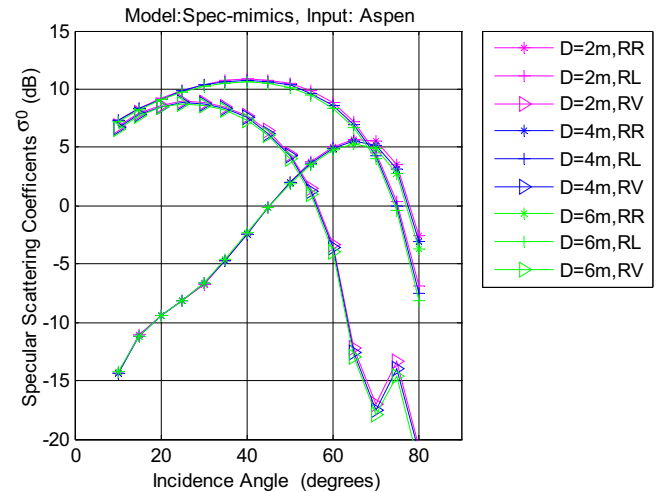


Fig. 7. Specular scattering coefficients of different polarizations (RR, RL and RV) vs. specular incidence angles at different crown depths (8, 10 and 12 m).

scattering at the specular directions are stronger than the other directions, as the development of GNSS-R receiver, such as the enhancement of the receiver's gain, it is believable that the in-coherent scattering at the other directions may be received someday. Therefore, we show the azimuth effects ( $\theta_i = \theta_s = 30^\circ$ ) on the out-of-plane bistatic scattering. We can easily see from Fig. 8 that the azimuth symmetry of scattering due to the model assumption. When the azimuth angle is lower than  $120^\circ$ ,  $RL > RV > RR$ , the RR is the smallest and has the lowest scattering ( $\varphi_s = 30^\circ$ ). When  $120^\circ < \varphi_s \leq 180^\circ$ ,  $RL > RR > RV$ . RL and RV decrease as the increase of azimuth angles ( $50^\circ \leq \varphi_s \leq 180^\circ$ ), but the RR first decreases with  $\varphi_s \leq 30^\circ$  and then increase with  $30^\circ \leq \varphi_s \leq 50^\circ$ . From the above simulations, we can see the scattering azimuth angles effects are very important for the final scattering trends.

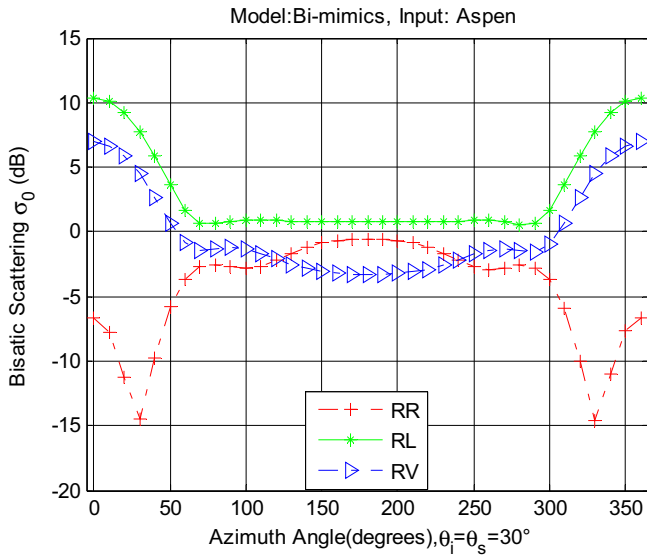


Fig. 8. Bistatic scattering vs. scattering azimuth angles ( $\theta_i = \theta_s = 30^\circ$ ) at different polarizations (RR, RL and RV).

**5. Conclusions**

To overcome the ionospheric effect, the GNSS transmitted signals are RHCP. After reflecting from the Earth surface, its polarization is mostly swapped, which is commonly thought that the signals are flipped to LHCP, however this flipped polarization properties are not well understood at present. But in fact, the flipping extent is depending on the surface’s dielectric properties. The polarization scattering mechanism for GNSS-R vegetation remote sensing is addressed in our work. The Bi-mimics model is used in this paper. The Spec-mimics model is used according to the GNSS-R configuration. Specular circular scattering properties are simulated, including co-polarization and cross-polarization. Specifically, the VR, HR, +45R and -45R are all included in the cross-polarization simulations except for the commonly used LR polarization. Theoretical calculations indicate that RR polarization exists for the entire incidence angle range, but it is the smallest for smaller incidence angles ( $\theta \leq 50^\circ$ ). Contributions of different components at RR, LR and VR polarization are also simulated. The total trunk component is existed for the entire incidence angle range and dominates the total scattering (RR, LR and VR polarization), while the total crown component has much less effects. The VR has dips for larger incidence angles ( $70^\circ$ ). As considered for retrieval, the VR polarization component should also be considered. Different trunk heights affect the scattering amplitudes of RR, LR and VR but have no effects on the scattering trend. Crown depths has a little effect on the scattering of RR, LR and VR. Meanwhile, the angle response of co-polarization and cross-polarization should also be considered carefully, and the azimuth angle has effects on the scattering of different polarizations. The influence of polarization on GNSS-R scattering is an interesting issue, because the

polarization information would provide the potential utility in terrestrial objects detections. In the future, it needs to further study and test.

**Acknowledgments**

The work is supported by Open Fund of State Key Laboratory of Remote Sensing Science (Grant No. OFSLRSS201010), Natural Science Foundation of the Inner Mongolia Autonomous Region (Grant No. 2013MS0602), National Basic Research Program of China (973 Program) (Grant No. 2012CB720000), Main Direction Project of Chinese Academy of Sciences (Grant No. KJCX2-EW-T03), and National Natural Science Foundation of China (NSFC) Project (Grant Nos. 11173050 and 11373059). Thanks very much for the advisable suggestions given by Prof. Jiancheng Shi at the State Key Laboratory and Prof. Yang Du at Zhejiang University. Also, it is extremely grateful to the reviewers’ very useful comments on the manuscript.

**Appendix A**

DDM	Delay-Doppler Maps
GPS	Global Positioning System
GNSS	Global Navigation Satellite Systems
GNSS-R	GNSS-Reflectometry
LHCP	Left Hand Circular Polarization
Mimics	Michigan Microwave Canopy Scattering Model
RHCP	Right Hand Circular Polarization
RR	The polarization of the transmitted signal is RHCP, while the received one is also RHCP
LR	The polarization of the transmitted signal is RHCP, while the received one is LHCP
Co-polarization	The polarization of the transmitted and received signals are the same
Cross-polarization	The polarization of the transmitted and received signals are different
HR, VR, +45R and -45R polarizations	The polarization of the transmitted signals are RHCP with the received ones H (horizontal), V (vertical), +45 (+45° linear) and -45 (-45° linear) polarizations, respectively

SMIGOL	Soil Moisture Interference pattern GNSS Observations at L-band Reflectometer
Z–V model	Zavorotny–Voronovich model
SMEX	Soil Moisture Experiments

## References

- Beckmann, P., Spizzichino, A., 1987. *The Scattering of Electromagnetic Waves from Rough Surfaces*. Artech House, Norwood, MA, USA.
- Cardellach, E., Fabra, F., Nogués-Correig, O., Oliveras, S., Ribó, S., Rius, A., 2011. GNSS-R ground-based and airborne campaigns for ocean, land, ice, and snow techniques: application to the GOLD-RTR data sets. *Radio Sci.* 46, RS0C04. <http://dx.doi.org/10.1029/2011RS004683>.
- Clarizia, M., Gommenginger, C., Di Bisceglie, M., Galdi, C., Srokosz, M.A., 2012. Simulation of L-Band bistatic returns from the ocean surface: a facet approach with application to ocean GNSS reflectometry. *IEEE Trans. Geosci. Remote Sens.* 50, 960–971.
- Egido, A., Caparrini, M., Ruffini, G., Paloscia, S., Santi, E., Guerriero, L., Pierdicca, N., Floury, N., 2012. Global navigation satellite systems reflectometry as a remote sensing tool for agriculture. *Remote Sens.* 4 (8), 2356–2372.
- Ferrazzoli, P., Guerriero, L., Pierdicca, N., Rahmoune, R., 2010. Forest biomass monitoring with GNSS-R: theoretical simulations. *Adv. Space Res.* 47 (10), 1823–1832. <http://dx.doi.org/10.1016/j.asr.2010.04.025>.
- Gleason, S.C., Gommenginger, Cromwell, D., 2009. Fading statistics and sensing accuracy of ocean scattered GNSS and altimetry signals. *Adv. Space Res.* 46 (2), 208–220.
- Jin, S.G., Komjathy, A., 2010. GNSS reflectometry and remote sensing: new objectives and results. *Adv. Space Res.* 46 (2), 111–117. <http://dx.doi.org/10.1016/j.asr.2010.01.014>.
- Jin, S.G., Feng, G., Gleason, S., 2011. Remote sensing using GNSS signals: current status and future directions. *Adv. Space Res.* 47 (10), 1645–1653. <http://dx.doi.org/10.1016/j.asr.2011>.
- Liang, P., Pierce, L.E., Moghaddam, M., 2005. Radiative transfer model for microwave bistatic scattering from forest canopies. *IEEE Trans. Geosci. Remote Sens.* 43, 2470–2483.
- Martin-Neira, M., 1993. A passive reflectometry and interferometry system (PARIS): application to ocean altimetry. *ESA J.* 17, 331–355.
- Masters, D., Axelrad, P., Katzberg, S., 2004. Initial results of land-reflected GPS bistatic radar soil moisture measurements in SMEX02. *Remote Sens. Environ.* 92, 507–520.
- Rodriguez-Alvarez, N., Bosch-Lluis, X., Camps, A., Vall llossera, M., Valencia, E., Marchan-Hernandez, J., Ramos-Perez, I., 2009. Soil moisture retrieval using GNSS-R techniques: experimental results over a bare soil field. *IEEE Trans. Geosci. Remote Sens.* 47 (11), 3616–3624. <http://dx.doi.org/10.1109/TGRS.2030672>.
- Rodriguez-Alvarez, N., Camps, A., Vall-llossera, M., Bosch-Lluis, X., Monerris, A., Ramos-Perez, I., Valencia, E., Marchan-Hernandez, J., Martinez-Fernandez, J., Baroncini-Turricchia, G., Pérez-Gutiérrez, C., Sanchez, N., 2011a. Land geophysical parameters retrieval using the interference pattern GNSS-R technique. *IEEE Trans. Geosci. Remote Sens.* 49 (1), 71–84. <http://dx.doi.org/10.1109/TGRS.2010.2049023>.
- Rodriguez-Alvarez, N., Bosch Lluis, X., Camps, A., Aguasca, A., Vall llossera, M., Valencia, E., Ramos Perez, I., Park, H., 2011b. Review of crop growth and soil moisture monitoring from a ground based instrument implementing the interference pattern GNSS-R technique. *Radio Sci.* 46, 03. <http://dx.doi.org/10.1029/2011RS004680>.
- Small, E.E., Larson, K.M., Braun, J.J., 2010. Sensing vegetation growth with reflected GPS signals. *Geophys. Res. Lett.* 37, 12401. <http://dx.doi.org/10.1029/2010GL042951>.
- Ulaby, F.T., Elachi, C., 1990. *Radar Polarimetry for Geoscience Applications*. Artech House Publishers, Norwood, MA, USA.
- Ulaby, F.T., Sarabandi, K., McDonald, K., Whitt, M., Dobson, M.C., 1990. Michigan microwave canopy scattering model. *Int. J. Remote Sens.* 11, 1223–1253.
- Wu, X.R., Li, Y., Li, C., 2012. Crop biomass monitoring using GNSS-R technique based on bi-mimics model. *Remote Sens. Technol. Appl.* 27 (2), 220–230.
- Wu, X.R., Li, Y., Xu, J., 2012a. Theoretical study on GNSS-R vegetation biomass. In: *IEEE International Geoscience and Remote Sensing Symposium (IGARSS)*, Munich, Germany, July 22–27.
- Zavorotny, V., Voronovich, A.G., 1999. Bistatic radar scattering from an ocean surface in the small-slope approximation. In: *IEEE Int. Geoscience and Remote Sensing Symposium*, Piscataway, NJ, June 28–July 2.
- Zavorotny, V., Voronovich, A.G., 2000a. Scattering of GPS signals from the ocean with wind remote sensing application. *IEEE Trans. Geosci. Remote Sens.* 38 (3), 951–964.
- Zavorotny, V.U., Voronovich, A.G., 2000b. Bistatic GPS signal reflections at various polarizations from rough land surface with moisture content. In: *IEEE International Geoscience and Remote Sensing Symposium*, Honolulu, Hawaii, July 24–28.